PHILOSOPHICAL TRANSACTIONS A

rsta.royalsocietypublishing.org

Research

Cite this article: Hilchenbach M *et al*. 2017 Mechanical and electrostatic experiments with dust particles collected in the inner coma of comet 67P by COSIMA onboard Rosetta. *Phil. Trans. R. Soc. A* **375**: 20160255.
http://dx.doi.org/10.1098/rsta.2016.0255

Accepted: 12 January 2017

One contribution of 14 to a discussion meeting issue 'Cometary science after Rosetta'.

Subject Areas:
solar system, space exploration

Keywords:
comet, dust, coma, fragmentation

Author for correspondence:
Martin Hilchenbach
e-mail: hilchenbach@mps.mpg.de

Mechanical and electrostatic experiments with dust particles collected in the inner coma of comet 67P by COSIMA onboard Rosetta

Martin Hilchenbach[1], Henning Fischer[1], Yves Langevin[2], Sihane Merouane[1], John Paquette[1], Jouni Rynö[3], Oliver Stenzel[1], Christelle Briois[4], Jochen Kissel[1], Andreas Koch[5], Rita Schulz[6], Johan Silen[3], Nicolas Altobelli[7], Donia Baklouti[2], Anais Bardyn[4,8], Herve Cottin[8], Cecile Engrand[9], Nicolas Fray[8], Gerhard Haerendel[10], Hartmut Henkel[4], Herwig Höfner[10], Klaus Hornung[11], Harry Lehto[12], Eva Maria Mellado[11], Paola Modica[4,8], Lena Le Roy[13], Sandra Siljeström[14], Wolfgang Steiger[15], Laurent Thirkell[4], Roger Thomas[3], Klaus Torkar[16], Kurt Varmuza[17], Boris Zaprudin[15] and the COSIMA team

[1]Max-Planck-Institut für Sonnensystemforschung, Justus-von-Liebig-Weg 3, 37077 Göttingen, Germany
[2]Institut d'Astrophysique Spatiale, CNRS/Université Paris Sud, Bâtiment 121, 91405 Orsay, France
[3]Finnish Meteorological Institute, Erik Palmenin aukio 1, PO Box 503, 00101 Helsinki, Finland
[4]Laboratoire de Physique et Chimie de l'Environnement et de l'Espace, CNRS/Université d'Orléans, 3 Av. de la Recherche Scientifique, 45071 Orléans, France
[5]von Hoerner und Sulger GmbH, Schlossplatz 8, 68723 Schwetzingen, Germany
[6]ESA – ESTEC, Postbus 299, 2200AG Noordwijk, The Netherlands
[7]Solar System Science Operation Division, ESA-ESAC, PO Box 78, 28691 Villanueva de la Cañada, Madrid, Spain

THE ROYAL SOCIETY PUBLISHING

[8]LISA, UMR CNRS 7583, Université Paris Est Créteil et Université Paris Diderot, Institut Pierre Simon Laplace, 94000 Créteil, France
[9]Centre de Sciences Nucléaires et de Sciences de la Matière - CSNSM, CNRS/IN2P3-Univ. Paris Sud (UMR8609), Université Paris-Saclay, Bat. 104, 91405 Orsay, France
[10]Max-Planck-Institut für Extraterrestrische Physik, Giessenbachstrasse, 85748 Garching, Germany
[11]Universität der Bundeswehr LRT-7, Werner Heisenberg Weg 39, 85577 Neubiberg, Germany
[12]Department of Physics and Astronomy, Tuorla Observatory, University of Turku, Väisäläntie 20, 21500 Piikkiö, Finland
[13]Center for Space and Habitability (CSH), University of Bern, Sidlerstrasse 5, 3012 Bern, Switzerland
[14]Department of Chemistry, Materials and Surfaces, SP Technical Research Institute of Sweden, PO Box 857, 50115 Borås, Sweden
[15]RC Seibersdorf Research GmbH Business Field Aerospace Technology, 2444 Seibersdorf, Austria
[16]Space Research Institute, Austrian Academy of Sciences, Schmiedlstrasse 6, 8042 Graz, Austria
[17]Institute of Statistics and Mathematical Methods in Economics, Vienna University of Technology, Wiedner Hauptstrasse 7/105-6, 1040 Vienna, Austria

MH, 0000-0003-1703-7777

The *in situ* cometary dust particle instrument COSIMA (COmetary Secondary Ion Mass Analyser) onboard ESA's Rosetta mission has collected about 31 000 dust particles in the inner coma of comet 67P/Churyumov–Gerasimenko since August 2014. The particles are identified by optical microscope imaging and analysed by time-of-flight secondary ion mass spectrometry. After dust particle collection by low speed impact on metal targets, the collected particle morphology points towards four families of cometary dust particles. COSIMA is an *in situ* laboratory that operates remotely controlled next to the comet nucleus. The particles can be further manipulated within the instrument by mechanical and electrostatic means after their collection by impact. The particles are stored above 0°C in the instrument and the experiments are carried out on the refractory, ice-free matter of the captured cometary dust particles. An interesting particle morphology class, the compact particles, is not fragmented on impact. One of these particles was mechanically pressed and thereby crushed into large fragments. The particles are good electrical insulators and transform into rubble pile agglomerates by the application of an energetic indium ion beam during the secondary ion mass spectrometry analysis.

This article is part of the themed issue 'Cometary science after Rosetta'.

1. Introduction

After a 10-year journey ESA's cornerstone mission Rosetta reached comet 67P/Churyumov–Gerasimenko (hereafter 67P) in August 2014. Since then Rosetta has been escorting the comet nucleus and the Rosetta mission ended on 30 September 2016. While the comet travelled into and out of the inner Solar System, the Rosetta spacecraft has been steered as close as 6.8 km or as far as 1500 km from the nucleus [1]. The COmetary Secondary Ion Mass Analyser (COSIMA) is part of the *in situ* dust instrument science payload of Rosetta [2]. COSIMA sequentially exposed and imaged target assemblies and collected, imaged and analysed dust particles in the inner coma in the vicinity of the comet nucleus.

Cometary nuclei are thought to be remnants of the building blocks present at the formation of the Solar System. Cometary dust particles might have formed from the agglomeration of particles present in the protosolar cloud or from presolar grains from previous generations of stars and part

of the material making up the protosolar nebula [3–6]. Cometary dust has been analysed *in situ* and by sample return by previous space missions such as Giotto and Vega to comet 1P/Halley or Stardust to comet 81P/Wild 2, and by investigations of various classes of micrometeorites and interplanetary dust particles in the laboratory. The relative velocity of the dust particles on braking and/or collection of about 70 and 6 km s^{-1} has been much higher than for the COSIMA instrument collection and the cometary particles have been either destroyed or severely altered in most cases [7,8]. The kinetic energy deposited by the dust particles during collection was about 6–8 orders of magnitude less during the COSIMA dust particle collection as the Rosetta spacecraft speed relative to the nucleus is about 1 m s^{-1} or less and the cometary dust particle speed in the inner coma of 67P is of the order of 10 m s^{-1} [9,10].

The dust particles collected by COSIMA are classified in four distinct morphological classes based on the images taken after their collection by low speed impact on metal targets. The observed particle typology and fragmentation morphologies are (i) compact, (ii) glued cluster, (iii) shattered cluster, and (iv) rubble pile cluster agglomerates [11]. Both particle material strength and impact speed determine the classification and cannot be disentangled without further experiments. The cometary particles are altered by the secondary ion mass spectrometry analysis and whole or parts of the particles are displaced or removed. For the cluster particles, the analysis of the composition has been possible in most cases as only a fraction of the particle was either removed or reshuffled and the particles seem to be heterogeneous in composition and morphology [12]. But compact particles could not be analysed successfully in the nominal mission phase of Rosetta as these particles are completely dislodged from the metal targets by exposure to the ion beam and/or the electric field applied during the analysis with the COSIMA's secondary ion mass spectrometer.

The shattered cometary dust particles are composed of subgrains that are tens of micrometres in diameter [13]. The interaction of the cometary particles with the spacecraft electric field due to its potential of the order of up to −20 V has been described as a process potentially causing the disruption of cometary dust particles prior to collection and/or detection resulting in particle showers as the particles approach the negative potential of the spacecraft [14]. Dust particles and surfaces being exposed to the local plasma, electrical and magnetic fields and solar radiation are charged and interact with the local plasma environment by a balance of the various charging currents [15]. Dust particle charging is assumed to cause cometary particle fragmentation in the coma, but has not been observed in the dust particle fluxes of comet 67P [12,16]. The capacity and electrical conductivity of dust particles are material properties applied in the modelling of dust–plasma interactions and the potential ejection of dust particles due to electrostatic forces from the nucleus surface [17,18].

In the following, we will describe and discuss experiments carried out on cometary particles captured in the inner coma of 67P within the COSIMA instrument. The particles are either pressed by mechanical means and/or bombarded with an energetic indium ion beam.

2. Material and methods

The instrument design and nominal operation modes are described in [2]. In the time period of interest, COSIMA collects cometary dust particles on porous Au metal targets. Three targets, with an area of 1 cm^2 each, are mounted together on one target holder. They are exposed for up to several months in the inner coma and the collected dust particles are imaged by an optical microscope (COSISCOPE) in time intervals in the range of half a day to several weeks. Owing to the porous Au top layer, the targets appear black in the microscopic images. The target temperature is up to 10°C as the COSIMA instrument is residing within the Rosetta spacecraft thermal insulation and is thermally controlled. Therefore, no ices can be observed by COSIMA. For each target, two images are recorded, with illumination at incident angles in the range of 5°–15° from the left and the right side. The dust particles are identified by the cast shadow and the light scattered off towards the microscope camera. For the porous gold targets, the reflectivity is less than 3% and the targets appear black. The COSIMA targets are identified by

a unique hex code ranging from XC0 to XD8. The X is substituted by the numbers 1, 2 or 3, indicating the top, mid and low position, respectively, of the target mounted on the targetholder. The images are subjected to either lossy or lossless compression. Further, for some images, subpixel resolution of 10 µm is available [11]. Nominally, particles of about 14 µm (COSISCOPE pixel size) can be identified and are specified by their coordinates in the target plane and the timestamp of the first image after their collection. The particles are named for individual tracking and bookkeeping.

Time-of-flight secondary ion mass spectrometry (TOF-SIMS) is applied to analyse the particle surface layers and the target background. The mass resolution $m/\Delta m$ in the period of interest is about 900 at half peak maximum at $m/z = 100$ u, thus allowing COSIMA to distinguish elements from organic molecules around the same integer mass for $m/z < 100$ u. The mass resolution is lower than the nominal value of about 1400. The footprint area of the primary indium ion beam is 1750 µm^2 and the pulse width is 6 ns (full width at half maximum). The energy of the primary In^+ is 8 keV and the In^+ beam pulses are compressed and shaped by a chopper/buncher. SIMS instrumental parameters have to be automatically optimized onboard prior to each SIMS measurement or scan matrix block. The mass spectrometer can detect either positive or negative secondary ions by reversing the potential of 3 kV of the secondary ion lens (SIL) in front of the mass spectrometer for either positive or negative SIMS mode. The distance between the SIL mounting plate and the target plane is 3 mm with the exception of the secondary ion collection hole which is drilled in a cone of 1 mm inner diameter, 1.2 mm outer diameter and a height of 1 mm, resulting in a 2 mm distance between the actual SIL and the plane target. The metal target is always electrically grounded. The electric field is 1.5 kV mm^{-1} or 1.5 V µm^{-1} next to the SIL cone and 1 V µm^{-1} off the SIL cone. In positive SIMS mode, the applied electric field accelerates positive secondary ions towards the mass spectrometer and the electric field is directed off the target. In negative TOF-SIMS mode, the negative secondary ions as well as electrons are accelerated towards the mass spectrometer and the electric field is directed towards the target. The positions to be analysed by TOF-SIMS are selected on the target and/or the particles. The in-plane target coordinates X, Y are derived from the images and the particle height Z is estimated from the cast shadow of the particle. As the flux of the collected secondary ions from the target is about 20× higher than from the particles, spectra collected on the particle surfaces and spectra collected on the target are summed and normalized to the Au elemental peak intensity for comparison.

The handling of the targetholder within the instrument is carried out by a three-dimensional robotic positioning unit, the so-called target manipulation unit (TMU). It moves the targetholder to the expose-position behind the COSIMA dust funnel for collection of dust particles, or moves it into storage, or places the individual targets on the targetholder in the focal plane of the microscope or single particles in front of the primary ion beam and the secondary ion mass spectrometer. The TMU handles all these different tasks including the exact positioning, across several centimetres as well as in tiny steps down to 0.8 µm along the x-, y- and z-axis and rotations up to 270° in 90° steps. One new function, not covered by the original task list to be carried out by the TMU, is the pressing (not necessarily crushing) of cometary particles towards the target plane. The rationale is that some particles, particularly the compact particles, can be lifted or dislodged from the target plates during the TOF-SIMS operation, preventing the analysis of their compositions. Slight pressing should ensure that the particles stick to the target during the TOF-SIMS analysis. Instead of moving the target nominally to storage, the target is positioned in front of the backside of another target in the storage and faces a flat, milled aluminium block with an area of 0.5×0.5 cm^2 with a surface roughness < 6.4 µm. The latter has the nominal function to ensure the precise positioning of the targetholder in the grip of the TMU robot. The TMU grip with the target moves on average about 0.5 mm s^{-1} along the z-axis towards the aluminium block or 2 mm within 3.8 s. Before the particle on the target is touched, the velocity is even lower since the TMU motion control loop decelerates before the final position is reached. The commanded distance along the z-axis defines how much the cometary particle will be pressed between the aluminium block and the metal target. The TMU grip with the targetholder is retracted after

about 60 s and nominal TMU operation is resumed. Part of the particle will stick to the metal target and another might stick to the plane surface of the aluminium block. The relative position of the aluminium block opposite to the target plane is known with an accuracy of about 0.1 mm and with a precision better than 15 µm. For the pressing of a particle, the commanded target grip position has been set to an envisaged gap of 120 µm between the target and the aluminium block on the backside of targetholder C7; the accuracy has been confined to about 50 µm by preceding dry runs before pressing the particle of interest.

A nominal TOF-SIMS spectrum lasts about 2.5 min and consists of 225 000 individual primary ion beam shots with the primary beam shot frequency being about 1.5 kHz. The mean current is estimated to be about 7 nA cm^{-2}. Two consecutive TOF-SIMS spectra are collected at the same position. Dust particles on two targets analysed by TOF-SIMS are illustrated and labelled by their name in figure 1. On the porous Au target 1D0, 140 spectra have been collected for each negative and positive matrix of TOF-SIMS scans next to and on the particle named Andrzej. There are 212 spectra each for matrix TOF-SIMS scans for the particle named Sigrid and 10 spectra each for the target position as a control or background measurement (figure 1*a*). On the porous Au target 1C3, a series of short duration negative mode TOF-SIMS analyses have been carried out on one spot on the surface of the particle named Lou with 220–225 000 primary ion beam shots as well as on a target position for the automatic on-board optimization of the TOF-SIMS parameters. Each sequence lasts for about 40 min including the TOF-SIMS, imaging and recalibration of the TOF-SIMS parameters. The particles of interest, named Eylem, Evren, Matthias and Lou, and the two TOF-SIMS positions are labelled in figure 1*b*. The TOF-SIMS coordinates as commanded for the negative TOF-SIMS spot on the particle Lou are shown in figure 1*c*. The accuracy of the TOF-SIMS position is about 50 µm in the *x*–*y* plane and along the *z*-axis. Shadowing effects of the particle topography, and the primary beam inclination due to the local electric field might add a further shift of the TOF-SIMS primary ion beam position relative to the particle surface.

3. Observations and results

(a) Crushing a compact particle

The cometary dust particle Andrzej was collected in the time period 7–14 November 2014. The distance of the nucleus was about 10–30 km, and the collection period overlapped with the landing of Philae on 12 November 2014. Andrzej has an area of 4.3×10^4 µm^2 and a height of about 200 µm. Its morphology has been classified as compact. Sigrid was collected between 14 and 21 November 2014, at a distance from the nucleus of about 30 km. The particle Sigrid has an area of 6×10^4 µm^2 and a height of about 50 µm [11]. Between imaging the particle on 10 April 2016 (figure 2*a*) and 13 April 2016 (figure 2*b*), the particle Andrzej was pressed between the target and the aluminium block as described above. The pressing took place on 12 April 2016. About three quarters of the particle volume is not recovered in the ensuing image. The resulting area is about 3×10^4 µm^2 and the height is reduced to about 70 µm as visible by the shorter cast shadow. The particle Andrzej is broken up and disrupted, a single, compact particle sticking to the target and the other part or parts are either lost or sticking to the aluminium block. Particle Sigrid is not altered as the particle height is less than the minimum distance of target plane and aluminium block.

(b) Secondary ion mass spectrometry of a compact particle and a cluster particle

TOF-SIMS matrix scans of the particles Andrzej and Sigrid were carried out on 20 and 21 April 2016. Negative mode TOF-SIMS matrix scans of particle Andrzej resulted in the fragmentation of the remaining part of particle Andrzej (figure 2*c*). The compact particle is transformed into a rubble pile of about 25 µm in height and an increased area of about 5×10^4 µm^2. A few tiny fragments are scattered up to 250 µm off the rubble pile. The particle Sigrid, not scanned by the primary ion beam, but exposed to the electric field during the TOF-SIMS analysis, is not

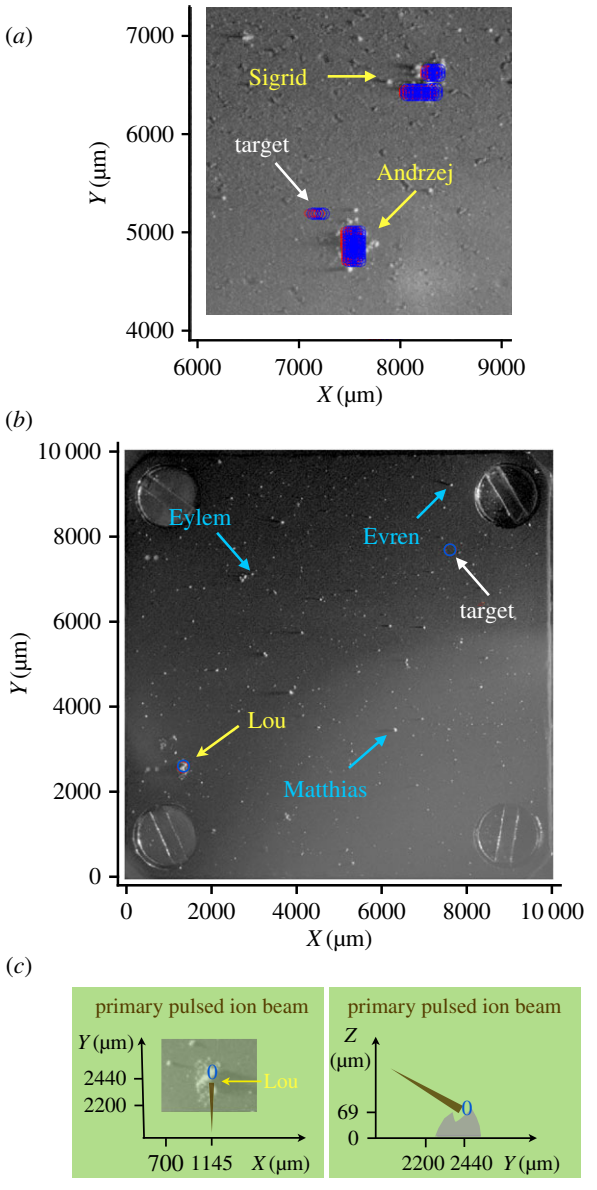

Figure 1. TOF-SIMS single and matrix scan positions on dust particles. (*a*) Sigrid and Andrzej on target 1D0; red and blue circles mark the positive and negative TOF-SIMS positions during the matrix scans of the particles and the target. (*b*) Lou, Eylem, Evren and Matthias on target 1C3; a blue circle marks the negative TOF-SIMS position during the sequential TOF-SIMS on Lou and target. (*c*) Particle Lou, primary ion beam direction (brown arrow) and intended footprint (blue circle) in target plane and versus schematic particle height profile as derived from Lou's cast shadow.

altered. Images of particle Andrzej after the ensuing positive mode TOF-SIMS matrix scans do not show any variation even for tiny particle fragments within the rubble pile (figure 2*d*). The glued cluster particle Sigrid is flattened to about 25 µm in height and has an almost unchanged area after the negative mode TOF-SIMS matrix scans. The morphology resembles a shattered cluster agglomerate (figure 2*e*). No stray particle fragments can be observed. Ensuing positive mode TOF-SIMS matrix scans on particle Sigrid do not show any further alterations, neither for particle Sigrid nor particle Andrzej (figure 2*f*).

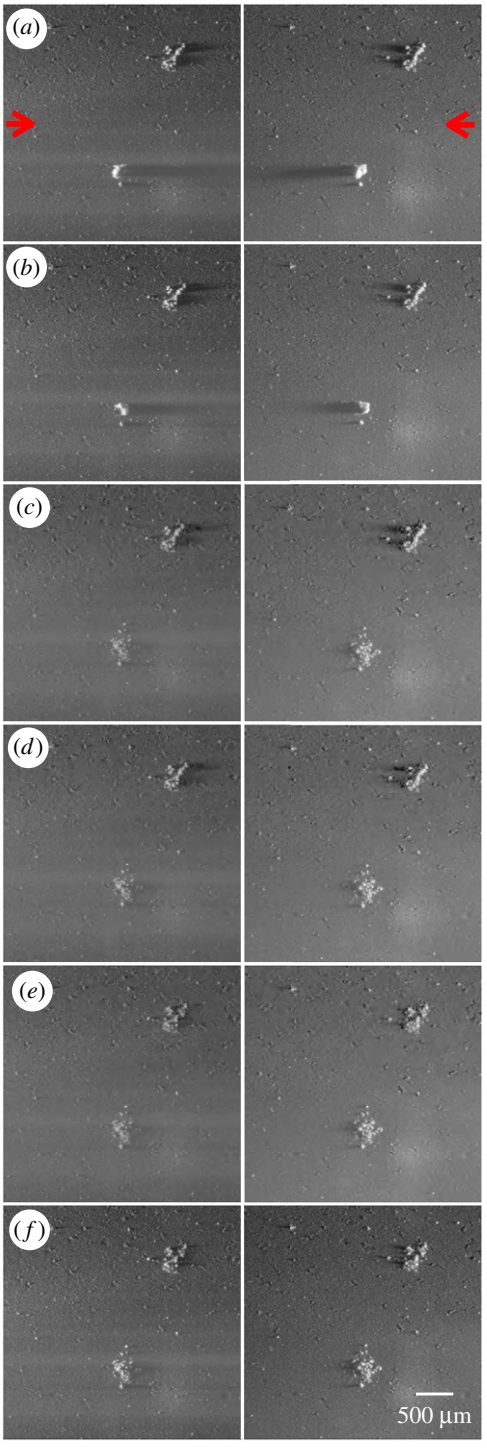

Figure 2. Optical microscope images (grazing incidence illumination indicated by red arrows) of particles Andrzej and Sigrid on target 1D0 (particle names and TOF-SIMS positions as labelled in figure 1). (*a*) Before mechanically pressing Andrzej. (*b*) After mechanically pressing Andrzej and a significant part of the particle is lost. (*c*) After negative matrix TOF-SIMS scans on Andrzej, the compact particle is transformed into a rubble pile. (*d*) After positive matrix TOF-SIMS scans on Andrzej. (*e*) After negative matrix TOF-SIMS scans on Sigrid, the glued cluster transformed into a shattered cluster agglomerate. (*f*) After positive matrix TOF-SIMS scans on Sigrid.

Positive TOF-SIMS secondary mass spectra of the particles Andrzej and Sigrid as well as the TOF-SIMS of the metal Au target are shown in figure 3. For particle Andrzej 70 spectra are selected and summed, for particle Sigrid 26 spectra and for the target 10 spectra. With the primary ion beam targeted on the same coordinate for two consecutive TOF-SIMS spectra, the ratios of the elemental peak intensities of the first and the second TOF-SIMS measurement showed only variations within the range expected from counting statistics and the two consecutive shots give rise to the same secondary ion yield. Thus the equilibrium for the secondary ion sputter and detection efficiency during TOF-SIMS has to be reached well within the time interval of 2.5 min for each secondary ion mass spectrum. The spectra are normalized for the Au elemental peak for comparison. Both particles are enriched for elements such as C, Na, Al, Mg, Si, S, K, Ca, Cr and Fe compared to the target background (figure 3*a*). Example mass spectra for integer masses 39 and 40 such as ^{39}K and ^{40}Ca and integer masses 54 to 58 such as ^{54}Fe, ^{56}Fe and FeH are shown in figure 3*b*,*c*. The target spectra are rich in hydrocarbons and polydimethylsiloxane compounds, and are attributed to terrestrial, spacecraft and/or instrument contamination. These compounds are much reduced on the particles. For comparison of the elemental composition of both particles, Andrzej and Sigrid, the particle secondary ion elemental peak intensities are normalized to Fe. No calibration was applied. The secondary ion peak ratios are similar for the glued cluster particle Sigrid and the compact fragment of particle Andrzej within elemental ratio variations of about 60%. The C and Si secondary ion peak ratios, as normalized to their respective Fe peak intensities, are about 40% lower on the compact fragment of particle Andrzej than on the glued cluster particle Sigrid (figure 3*d*). The average elemental peak ratios for Mg, Al, S and Cr are decreased, and Na, K and Ca are enhanced in particle Andrzej, but the error bars for these peak ratios are too large to be distinguished on a statistically significant level.

(c) Short duration secondary ion mass spectrometry of a cluster particle

The alterations observed for particles Sigrid and Andrzej have been observed only after an extended TOF-SIMS matrix scan. Therefore, for a particle, Lou, which has not been exposed to the primary ion beam before, the negative TOF-SIMS has been carried out on much shorter time scales and with only one position on the particle within the footprint of the primary ion beam. The dust particle Lou was collected between 19 and 20 May 2016 at distance of about 8 km from the comet nucleus centre. It has an area of 4.7×10^4 µm^2 and a maximum height of about 70 µm. The morphology is classified after impact as a glued cluster agglomerate.

On 5 June 2016, the negative mode TOF-SIMS was carried out in a sequence with 220, 220, 220, 879, 3516, 14 069, 56 250 and 225 000 primary indium beam pulses per TOF-SIMS spectrum. The time for one sequence consisting of initial spectra on the particle, the ensuing imaging and parameter optimization scan on the target for the TOF-SIMS parameters take about 50 min. The resulting secondary ion counts for the elemental peaks of H, C and O are shown in figure 4*a*. Within statistical error, the first three TOF-SIMS spectra with the same number of shots are similar. The secondary ion peak intensity is increasing with the number of shots summed per TOF-SIMS spectrum for the fourth and fifth TOF-SIMS spectra. This applies also for the sixth, seventh and eighth TOF-SIMS spectra, but alterations are observed between the fifth and sixth TOF-SIMS spectra: the H peak intensity is less than expected from extrapolation from the previous measurements, while for C and O this deviation is still within the statistical limits. Except for this deviation, the peak intensities scale with the number of primary ion beam shots per TOF-SIMS spectrum. The images of the target 1C3 on 3 June 2016 reflect the particles on the target before the TOF-SIMS; the image taken on 6 June 2016 shows the situation after the TOF-SIMS on particle Lou. Three particles in the size range of 40–80 µm equivalent diameter and casting long shadows, Eylem, Evren and Matthias, are lost. Particle Lou is altered slightly in the upper corner next to the footprint of the primary ion beam (figure 4*b*). The exact time of the loss of the three particles cannot be determined as only subsections of the images next to particle Lou and the SIMS target position between the TOF-SIMS sequences have been transferred due to limitations in the telemetry data rate. The sequential image series for particle Lou are shown in figure 5. No

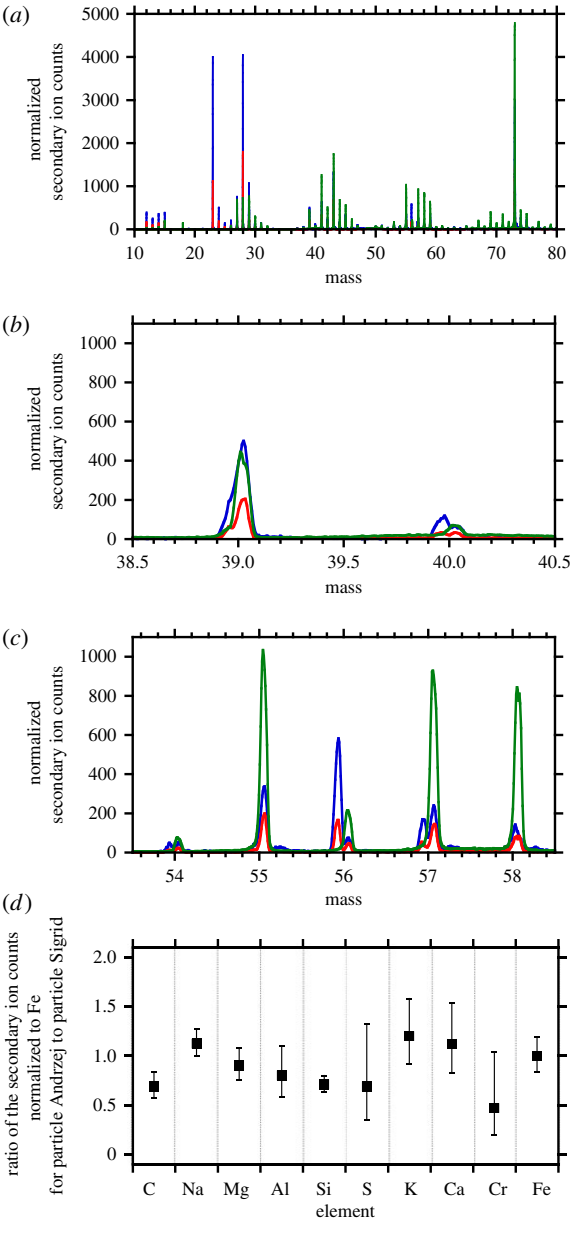

Figure 3. Positive secondary ion mass spectra (TOF-SIMS) for particles Andrzej (blue), Sigrid (red) and Au target (green), normalized to the respective elemental Au peak intensity. (*a*) Spectra in the mass range 10–80 u. (*b*) Spectra in the mass range 38.5–40.5 u including K and Ca. (*c*) Spectra in the mass range 53.5 to 58.5 u including Fe. (*d*) Ratio of secondary ion peak intensities normalized to Fe of particle Andrzej relative to particle Sigrid. Elements C and Si are depleted in the compact particle Andrzej relative to the glued cluster agglomerate Sigrid. Error bars refer to 68% confidence level for the statistical error.

alterations are observed up to sequence number 5 or 3516 shots. Then some additional particles are observed on the target next to the upper right corner of the particle Lou after sequence number 6 or 14 069 shots. No obvious alterations are visible for the following sequence number 7 or 56 250 shots. After the last TOF-SIMS with about 225 000 shots, or sequence number 8, several tiny particles are observed next to the upper right corner up to 300 µm off particle Lou along the *x*-axis. Further, more fragments are added to the ones next to the upper right corner, even piling

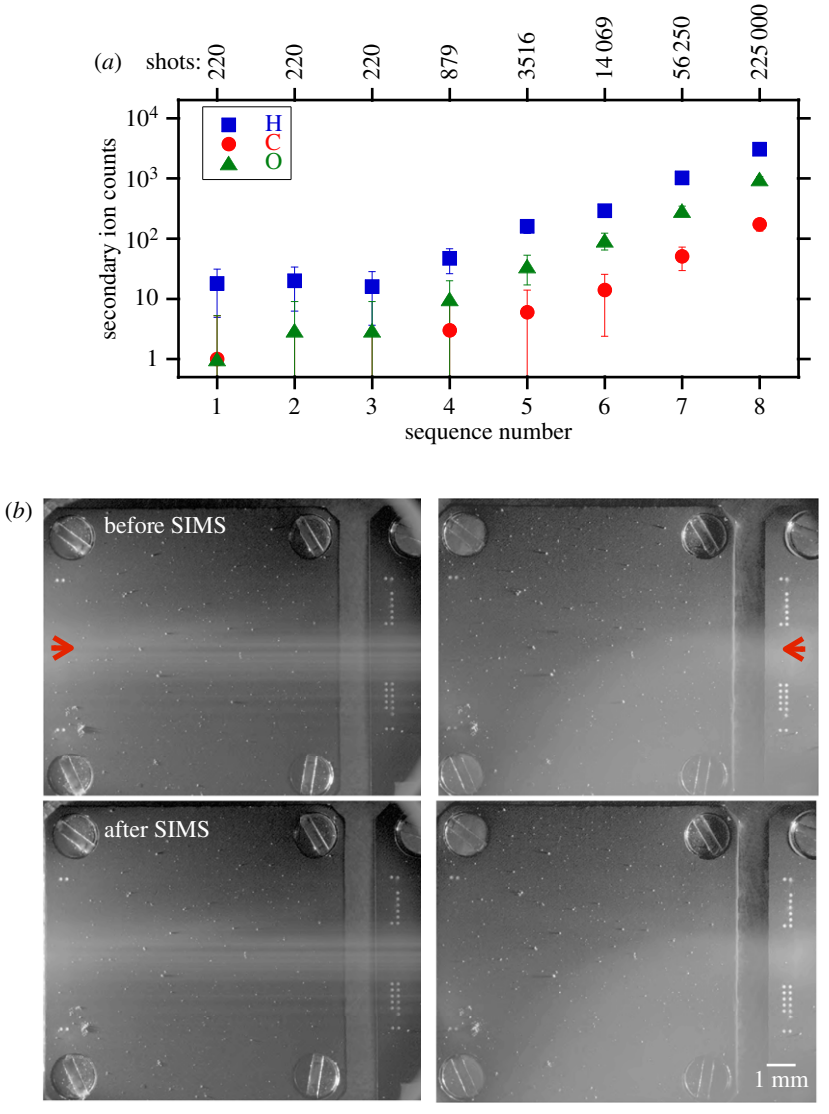

Figure 4. Secondary ion mass spectra measurements on particle Lou on target 1C3. (*a*) Sequential negative TOF-SIMS with the total ion counts for hydrogen H (blue), carbon C (red) and oxygen O (green), versus the sequence in time. Number of primary ion beam shots for each sequence indicated on top. Error bars refer to the 99% confidence level for the statistical error. (*b*) Optical microscope images (grazing incidence illumination indicated by red arrows) before and after the SIMS scans on target 1C3. Particles Eylem, Evren and Matthias are lost and particle Lou is altered (particle names are labelled in figure 1*b*).

up and casting a shadow indicating a height of 20 µm while the height of particle Lou is reduced as indicated by its cast shadow. Other particles in the vicinity of particle Lou are not affected and no alterations are spotted.

4. Discussion

The morphological classes of the cometary particles after impact on the COSIMA targets have been outlined based on the COSISCOPE images [11]. Alterations of the dust particles due to the TOF-SIMS analysis have been observed in the early mission phase and were attributed to the weak attachment of the particles to each other and to the target [12].

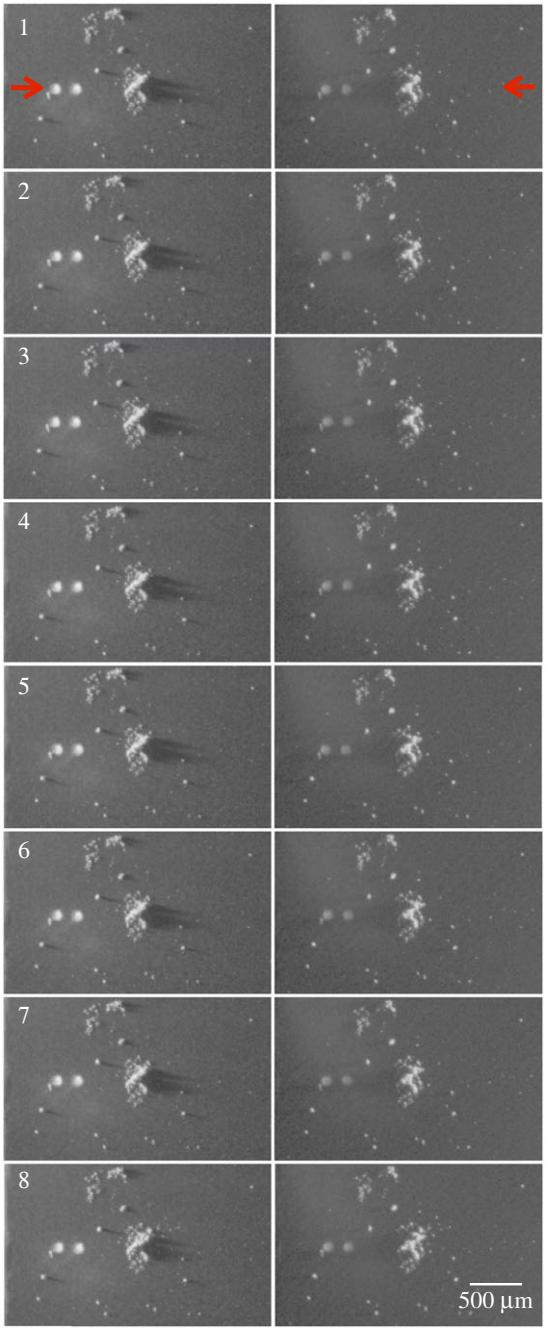

Figure 5. Optical microscope images (grazing incidence illumination indicated by red arrows, TOF-SIMS positions as labelled in figure 1*b*,*c*) of particle Lou on target 1C3 for the sequence of negative TOF-SIMS spectra collected from one spot on particle Lou and various numbers of primary beam ion shots. (1) After 220 shots, (2) after 220 shots, (3) after 220 shots, (4) after 879 shots, (5) after 3516 shots, (6) after 14 063 shots. Grains shifted next to right upper corner of Lou. (7) After 56 250 shots and (8) after 225 000 shots. About eight small grains shifted up to 300 µm off particle Lou and further rearrangements next to the right upper corner. None of the single particles next to Lou are removed.

Van der Waals forces are assumed to be the major forces for holding the particle agglomerate together as well as the sticking of the particles to the metal targets. The compact particle Andrzej is fractured and broken up by shear forces on compression between the two metal planes. The

part sticking on the target after the crushing is classified as a compact particle and no additional smaller fragments are observed on the target. The particle might have been damaged and there might be fractures and cracks at a spatial scale below the resolution of the COSISCOPE images, but that is analogous to all other observations of particles after collection by impact [13]. The remaining large chunk of the particle after the crushing is a strong hint that the particle shear strength is relatively high compared to other particles classified as cluster agglomerates and in line with the strength analysis for these particle classes [13,19].

The TOF-SIMS secondary mass spectrum of the compact fragment of particle Andrzej is similar to the glued cluster particle Sigrid except for its depletion in C and Si secondary ion intensities normalized to their respective Fe intensities. If the compact fragment of particle Andrzej is representative for the morphology class of compact particles, then these compact particles give rise to lower carbon and silicon intensities relative to iron than particles smashed and broken up on impact during the particle capture on the target and classified as cluster agglomerates.

The next series of experiments with cometary particles within the COSIMA instrument addresses the relevance of the electrostatic forces and the diverse range of the morphologies of the collected cometary particles within the footprint of the primary ion beam. The electrostatic forces acting on a non-conducting or insulating particle on a conducting substrate are: (i) attraction between the net charge on the particle and its image charge, (ii) the electric field acting on the particle charge or the Lorentz force, and (iii) the attraction between the field-induced dipole and its dipole image. The attracting forces scale with the square of the charge and the electric field while the Lorentz force is a function of the product of the charge and the electric field. The resulting quadratic equation defines the range of the charge of the particle and electric field for which the Lorentz force is more significant than the attracting electrostatic forces [20]. The electric field is the field between target and mass spectrometer entrance lens and the electric field due to neighbouring charged particles. Since the COSIMA primary ion beam consists of In^+ ions, the particles within the footprint of the primary ion beam are charged up positively during TOF-SIMS and this gives rise to a repulsive force between the charged particle elements. In the negative TOF-SIMS mode, the electric field is accelerating negatively charged particles such as negative ions and secondary electrons off the target while positively charged particles are driven towards the target. In negative TOF-SIMS mode and with the dust particles charged positively, all the electrostatic forces acting on a particle are directed towards the target and are compressing and/or shearing the particle with the exception of the repulsive forces due to the positive charge of neighbouring particles [21]. For positive TOF-SIMS mode, the adhesive forces are the same while the Lorentz force is directed off the target, potentially lifting the particle.

For electric field gradients, the third force or the field-induced dipole can lift particles by the dielectrophoretic forces, resulting in the particles being attracted to the electric field intensity maxima and repelled from its minima as the dielectric permittivity of the vacuum is smaller than the permittivity of the porous cometary matter [22,23]. For conducting particles, the field-induced charges on the conducting particles are separated and particles can be lifted in an external electric field [24]. Both forces do not require any seed charging of the particle by the primary ion beam or contact charging.

The morphology of the remnant of the compact particle Andrzej is transformed during negative mode TOF-SIMS matrix scan into a rubble pile agglomerate. The forces due to the TOF-SIMS were high enough to break up the compact particle. The size range of the fragments in the rubble pile is close to the particle size distribution reported for the rubble piles due to the particle impact on the target on collection and the resulting mechanical fragmentation. The TOF-SIMS operates in the static TOF-SIMS region, but still sufficient energy is transferred to the particle to cause disruption during the matrix TOF-SIMS scans. The particle is fragmented due to the electrical forces in the negative TOF-SIMS mode: charging due to the primary ion beam scanning across the particle and the external electric field applied for the transfer of the secondary ions to the mass spectrometer for analysis and detection. The volume of particle Andrzej has remained the same within the measurement uncertainties, the area covered by the particle is increased and the particle height is reduced. Across the particle, the electrical potential drops by about

300 V before the TOF-SIMS and about 70 V after the TOF-SIMS assuming the electric field to be a function of the particle height. Small, positively charged fragments, broken off the top of the particle, are accelerated in the electric field down towards the target and, similar to the particle impact on collection, are de-accelerated due to the rolling friction [25].

The negative TOF-SIMS mode matrix scan on the glued cluster particle Sigrid resulted in fragmentation of the particle and the ensuing classification as a shattered cluster agglomerate. Similar to Andrzej, this is most likely due to the electrical forces caused by the charging and the applied electric field. The fragments are less scattered and closer to the main particle and the resulting shattered cluster agglomerate appears to be flat. The shape of the particle Sigrid is altered, but the volume seems to be the same before and after the negative mode TOF-SIMS matrix scans, similar to Andrzej. Neither Andrzej nor Sigrid nor any other particle was fragmented or further fragmented just by the application of the electric field. The charging due to the primary ion beam is essential for particle fragmentation. Ensuing positive TOF-SIMS mode matrix scans did not visibly alter either particle morphology any further. This might be due to the fact that the particles have been already fragmented during the prior negative mode TOF-SIMS matrix scans and no further fragmentation could be caused by the ensuing positive TOF-SIMS mode matrix scans with the same primary ion beam settings.

The short negative TOF-SIMS mode sequential spectra on particle Lou revealed that the first visible alteration of the particle required between 3516 and 14 069 primary ion beam shots or the charge collected by the time of fracture being about 75–300 $\mu C\,m^{-2}$, based on a 7 $nA\,cm^{-2}$ primary ion beam current. After 250 000 shots a significant fragmentation is observed. The particle fragmentation has occurred next to the tip of the particle. This could be due to the tip of the particle being in the region of the primary ion beam footprint and/or the exposed position on the tip of the particle. Particle elements detach once the electrostatic repulsive forces are greater than the sum of the van der Waals forces and the electrostatic attracting forces. The fragment elements are further separated by acceleration along the static electrical TOF-SIMS field towards the target. The distance travelled by the tiny fragments can be explained by assuming rolling friction as the energy dissipative process. For spherical particles with a charge of up to 100 fC, a size of 14 μm diameter, a potential drop of 1.5 $MV\,m^{-1}$ across 70 μm and a density of about 0.5 $g\,cm^{-3}$, the distance range would be between 70 and 700 μm as a function of the rolling friction which is assumed to be a factor of 0.01–0.1 lower than the static friction [13]. The maximum distance observed is about 300 μm and within the expected range.

During the negative TOF-SIMS of particle Lou, the particles Eylem, Evren and Matthias are removed. These particles have not been charged by the primary ion beam. Other particles, similar in size and height or being much closer to the position of the charging primary ion beam during the TOF-SIMS are not lifted nor moved. The lifting force can be due to the dielectrophoretic force or the particles being negatively charged and then lifted in the applied external electric field. The dielectrophoretic force is not dependent on the particle charge or the polarity of the applied electric field, but depends on the field gradients and the particle permittivity relative to the embedding medium. The electric field gradients are only due to the particle sticking out on the target in an otherwise uniform electric field next to the target. The DC permittivity for porous particles without ices is estimated to be less than 1.3 relative to vacuum for 70 μm particles, and assumed to be even smaller for larger and porous cometary particles without ices, with the permittivity being a function of the particle porosity [26]. The adhesion due to van der Waals forces scales with the size of the particles. The dielectrophoretic forces do not explain the 'lifting' preference for the particle size range next to 50–100 μm equivalent diameter and 50 μm in height.

About 10 000 primary ion beam shots, spanning a time interval of about 6.6 s at 1.5 kHz, are sufficient to track visible particle fragmentation in the images of the particle Lou. The size distribution of the particle fragments is due to the size of the primary ion beam footprint of 35×50 μm^2 as the Coulomb force scales with the particle charges and the repulsive force has a maximum if the charges are equally distributed among the particle elements. We assume that all charges within the primary ion beam footprint are collected without significant loss during

the time interval of 6.6 s and estimate the capacitance of a spherical fragment particle element of 14 µm in diameter as 2 fF. Then the specific resistance of the particles is about $10^{16}\ \Omega\,\mathrm{mm}^2\,\mathrm{m}^{-1}$. The particles are good electrical insulators and their electric specific resistance is comparable with that of paper.

The particles can be charged by contact charging of the insulating particles adhering to the metal targets [27–29]. The applied electric field can lift a charged particle if it is charged negatively in the negative or positively in the positive mode TOF-SIMS. In the TOF-SIMS series of particle Lou, only negative mode TOF-SIMS was applied. The lifting or Lorentz force due to the applied electric field and the particle charge must be larger than the adhesion force to the target due to van der Waals forces and, potentially, electrostatic forces. In COSIMA, the charge necessary to detach the particle from the Au target is of the same order of magnitude as the charge to break up the particle or detach a particle element. Contact charging might give rise to up to about 10 $\mu\mathrm{C\,m}^{-2}$ [30,31] as compared to 75–300 $\mu\mathrm{C\,m}^{-2}$ for the particle fragmentation within COSIMA. The contact charge estimate is in line with the observation that particles are not fragmented by application of a high electric field and/or contact with the metal target as the resulting surface charge density is below the threshold to break up the particle. The charging due to the primary beam triggers the particle fragmentation. For a 70 µm diameter spherical particle, the upward force in the electric field in negative TOF-SIMS mode is about 30 nN due to an estimated contact charge of about −20 fC and applied electric field of $1.5\ \mathrm{V\,\mu m}^{-1}$. That is about 1% of the lower threshold for the particle adhesion force of about 2 µN, assumed to be only due to van der Waals forces and derived from 0.4 µN for a 14 µm sized particle and a linear dependence on the particle size [13,32–34]. Both forces scale with the particle size and do not explain the observed preferential lifting of particles larger than 50 µm. The electrostatic mirror force due to the dielectric particle attached to the conductive target would add to the adhesion force for larger particles. The lifting of a compact particle, elliptical in shape such as particle Matthias with a volume envelope of $35 \times 75 \times 45\ \mu\mathrm{m}^3$, might be accomplished along a dynamic pathway: the particle is first tilted or rolled due to the torque induced by the polarization by the electric field in the dielectric particle or due to non-isotropic charge distribution. The torque is proportional to the particle size. The adhesion force is reduced to low values as applied for rolling friction and the Lorentz force due to the contact charge could be sufficient to detach and lift the whole particle in the applied electric field. In the laboratory, mechanical vibration introduced a similar effect on toner particles and the uncertainty introduced by the range of the magnitudes of the van der Waals forces and the assumption of spherical particle shape and uniform charge distribution as compared to the real particle shape and non-uniform charge distribution can give rise to systematic errors of about one to two orders of magnitude for the ratio of the attraction to the repulsive forces acting on the particles [20]. This large variation might explain the observations that particles of similar size and shape are detached only in some cases by the application of the electrostatic field during TOF-SIMS.

5. Conclusion

The ice-free particles analysed after capture in the inner coma of 67P and storage within COSIMA at about 10°C have an electrical specific resistance of about $10^{16}\ \Omega\,\mathrm{mm}^2\,\mathrm{m}^{-1}$. This is of the same order as that of paper and these particles are good electrical insulators. The particles can be manipulated and fragmented either by mechanical means such as impact or crushing, or by charging them up. High electrostatic fields, such as $1.5\ \mathrm{MV\,m}^{-1}$, can lift larger particles off the gold targets without fragmentation of the particles. Cometary dust particles classified based on their morphology after impact on collection can be transformed by TOF-SIMS analysis from one morphology class to another one: compact particles to rubble piles as well as glued cluster to shattered cluster agglomerates. Both morphology classes reveal the elemental fragments and the compact and glued cluster particle agglomerates are assembled out of units in the tens of micrometre size range. The composition of the particles is heterogeneous and varies up to 60% for the observed secondary ion intensities normalized to iron between the two particles fragmented and analysed by positive TOF-SIMS matrix scans.

Authors' contributions. H.F., J.R. and O.S. designed and carried out the remote experiments, M.H. initiated the experiments and wrote the manuscript, O.S., S.M., J.P., J.R. and Y.L. provided the higher level data analysis tools, J.K., A.K., J.R., W.S., C.E., Ha.H., He.H., K.H., W.S., L.T., R.T., K.T., K.V. contributed to instrument development. H.F., J.R., O.S., M.H., C.B., H.C., C.E., N.F., H.L., P.M., S.S., L.T. contributed to instrument operations and J.R., J.P., O.S., S.M., P.M., A.B., N.F. to the data distribution. C.B., J.K., R.S., J.S., N.A., D.B., A.B., H.C., C.E., N.F., G.H., K.H., H.L., E.M., P.M., L.R., S.S., L.T., K.V., B.Z. contributed to data analysis. J.K. and M.H. are the two successive principal investigators of the COSIMA project. All authors discussed the results and commented on the manuscript.

Competing interests. We declare we have no competing interests.

Funding. No funding has been received for this article.

Acknowledgements. COSIMA was built by a consortium led by the Max-Planck-Institut für Extraterrestrische Physik, Garching, Germany, in collaboration with Laboratoire de Physique et Chimie de l'Environnement et de l'Espace, Orléans, France, Institut d'Astrophysique Spatiale, CNRS/Université Paris Sud, Orsay, France, Finnish Meteorological Institute, Helsinki, Finland, Universität Wuppertal, Wuppertal, Germany, von Hoerner und Sulger GmbH, Schwetzingen, Germany, Universität der Bundeswehr, Neubiberg, Germany, Institut für Physik, Forschungszentrum Seibersdorf, Seibersdorf, Austria, Institut für Weltraumforschung, Österreichische Akademie der Wissenschaften, Graz, Austria and is led by the Max-Planck-Institut für Sonnensystemforschung, Göttingen, Germany, with the support of the national funding agencies of Germany (DLR, grant no. 50 QP 1302), France (CNES), Austria, Finland and the ESA Technical Directorate. We thank the Rosetta project at ESTEC, the Rosetta Mission Operations Centre at ESOC and the Rosetta Science Ground Segment at ESAC for their outstanding work enabling the science return of the Rosetta Mission and making available the Rosetta science data to the public through the ESA Planetary Science Archive [35]. Rosetta is an ESA mission with contributions from its Member States and NASA.

References

1. Glassmeier K-H, Boehnhardt H, Koschny D, Kührt E, Richter I. 2007 The Rosetta mission: flying towards the origin of the solar system. *Space Sci. Rev.* **128**, 1–21. (doi:10.1007/s11214-006-9140-8)
2. Kissel J *et al.* 2007 Cosima high resolution time-of-flight secondary ion mass spectrometer for the analysis of cometary dust particles onboard Rosetta. *Space Sci. Rev.* **128**, 823–826. (doi:10.1007/s11214-006-9083-0)
3. Greenberg JM. 1998 Making a comet nucleus. *Astron. Astrophys.* **330**, 375.
4. Blum J, Gundlach B, Mühle S, Trigo-Rodríguez JM. 2014 Comets formed in solar-nebula instabilities—an experimental and modeling attempt to relate the activity of comets to their formation process'. *Icarus* **235**, 156–169. (doi:10.1016/j.icarus.2014.03.016)
5. Blum J, Gundlach B, Mühle S, Trigo-Rodríguez JM. 2015 Corrigendum to 'Comets formed in solar-nebula instabilities!—an experimental and modeling attempt to relate the activity of comets to their formation process'. *Icarus* **248**, 135–136. (doi:10.1016/j.icarus.2014.10.025)
6. Davidsson BJR *et al.* 2016 The primordial nucleus of comet 67P/Churyumov-Gerasimenko. *Astron. Astrophys.* **592**, A63. (doi:10.1051/0004-6361/201526968)
7. Jessberger EK, Christoforidis A, Kissel J. 1988 Aspects of the major element composition of Halley's dust. *Nature* **332**, 691–695. (doi:10.1038/332691a0)
8. Brownlee D. 2014 The Stardust mission: analyzing samples from the edge of the solar system. *Annu. Rev. Earth Planet. Sci.* **42**, 179–205. (doi:10.1146/annurev-earth-050212-124203)
9. Rotundi A *et al.* 2015 Dust measurements in the coma of comet 67P/Churyumov-Gerasimenko inbound to the Sun. *Science* **347**, aaa3905. (doi:10.1126/science.aaa3905)
10. Corte VD *et al.* 2015 GIADA: shining a light on the monitoring of the comet dust production from the nucleus of 67P/Churyumov-Gerasimenko. *Astron. Astrophys.* **583**, A13. (doi:10.1051/0004-6361/201526208)
11. Langevin Y *et al.* 2016 Typology of dust particles collected by the COSIMA mass spectrometer in the inner coma of 67P/Churyumov-Gerasimenko. *Icarus* **271**, 76–97. (doi:10.1016/j.icarus.2016.01.027)
12. Hilchenbach M *et al.* 2016 Comet 67P/Churyumov-Gerasimenko: close-up on dust particle fragments. *Astrophys. J.* **816**, L32. (doi:10.3847/2041-8205/816/2/L32)

13. Hornung K *et al.* 2016 A first assessment of the strength of cometary particles collected in-situ by the COSIMA instrument onboard ROSETTA. *Planet. Space Sci.* **133**, 63–75. (doi:10.1016/j.pss.2016.07.003)
14. Fulle M *et al.* 2015 Density and charge of pristine fluffy particles from comet 67P/Churyumov-Gerasimenko. *Astrophys. J.* **802**, L12. (doi:10.1088/2041-8205/802/1/L12)
15. Whipple EC. 1981 Potentials of surfaces in space. *Rep. Prog. Phys.* **44**, 1197–1250. (doi:10.1088/0034-4885/44/11/002)
16. Hill JR, Mendis DA. 1981 Electrostatic disruption of a charged conducting spheroid. *Can. J. Phys.* **59**, 897–901. (doi:10.1139/p81-116)
17. Mendis DA, Horanyi M. 2013 Dusty plasma effects in comets: expectations for Rosetta. *Rev. Geophys.* **51**, 53–75. (doi:10.1002/rog.20005)
18. Nordheim TA, Jones GH, Halekas JS, Roussos E, Coates AJ. 2015 Surface charging and electrostatic dust acceleration at the nucleus of comet 67P during periods of low activity. *Planet. Space Sci.* **119**, 24–35. (doi:10.1016/j.pss.2015.08.008)
19. Blum J, Schräpler R, Davidsson BJR, Trigo-Rodríguez JM. 2006 The physics of protoplanetesimal dust agglomerates. I. Mechanical properties and relations to primitive bodies in the Solar System. *Astrophys. J.* **652**, 1768–1781. (doi:10.1086/508017)
20. Feng JQ, Hays DA. 2003 Relative importance of electrostatic forces on powder particles. *Powder Technol.* **135**, 65–75. (doi:10.1016/j.powtec.2003.08.005)
21. Feng JQ. 2000 Electrostatic interaction between two charged dielectric spheres in contact. *Phys. Rev. E* **62**, 2891–2897. (doi:10.1103/PhysRevE.62.2891)
22. Jones TB. 2005 *Electromechanics of particles*. Cambridge, UK: Cambridge University Press.
23. Kofman W *et al.* 2015 Properties of the 67P/Churyumov-Gerasimenko interior revealed by CONSERT radar. *Science* **349**, aab0639. (doi:10.1126/science.aab0639)
24. Kok JF, Renno NO. 2008 The effects of electric forces on dust lifting: preliminary studies with a numerical model. *J. Phys. Conf. Ser.* **142**, 012047. (doi:10.1088/1742-6596/142/1/012047)
25. Kimura H, Wada K, Senshu H, Kobayashi H. 2015 Cohesion of amorphous silica spheres: toward a better understanding of the coagulation growth of silicate dust aggregates. *Astrophys. J.* **812**, 67. (doi:10.1088/0004-637X/812/1/67)
26. Rust AC, Russell JK, Knight RJ. 1999 Dielectric constant as a predictor of porosity in dry volcanic rocks. *J. Volcanol. Geothermal Res.* **91**, 79–96. (doi:10.1016/S0377-0273(99)00055-4)
27. Cho AYH. 1964 Contact charging of micron-sized particles in intense electric fields. *J. Appl. Phys.* **35**, 2561–2564. (doi:10.1063/1.1713799)
28. Sternovsky Z, Horányi M, Robertson S. 2001 Charging of dust particles on surfaces. *J. Vac. Sci. Technol. A* **19**, 2533–2541. (doi:10.1116/1.1392398)
29. Takeuchi M. 2006 Adhesion forces of charged particles. *Chem. Eng. Sci.* **61**, 2279–2289. (doi:10.1016/j.ces.2004.06.051)
30. Lowell J, Rose-Innes AC. 2006 Contact electrification. *Adv. Phys.* **29**, 947–1023. (doi:10.1080/00018738000101466)
31. Sternovsky Z, Robertson S, Sickafoose A, Colwell J, Horányi M. 2002 Contact charging of lunar and Martian dust simulants. *J. Geophys. Res. Planets* **107**, 5105. (doi:10.1029/2002JE001897)
32. Hoshino Y, Kiatkamjornwong S. 2007 Toner jumping phenomenon in an electric field. *Particul. Sci. Technol.* **25**, 147–162. (doi:10.1080/02726350701257667)
33. Hartzell CM, Scheeres DJ. 2011 The role of cohesive forces in particle launching on the Moon and asteroids. *Planet. Space Sci.* **59**, 1758–1768. (doi:10.1016/j.pss.2011.04.017)
34. Kimura H, Senshu H, Wada K. 2014 Electrostatic lofting of dust aggregates near the terminator of airless bodies and its implication for the formation of exozodiacal disks. *Planet. Space Sci.* **100**, 64–72. (doi:10.1016/j.pss.2014.03.017)
35. European Space Agency. 2017 Planetary Science Archive. http://www.cosmos.esa.int/web/psa/rosetta.